TRAJECTORY DYNAMICS IN THE EARTH-MOON SYSTEM

T. A. Heppenheimer †
Max-Planck-Institut für Kernphysik
Heidelberg, West Germany

Abstract

This paper constitutes a comprehensive overview of the main features of the dynamical problems associated with transport of lunar mass to a space colony via a catcher near the L_2 libration point. A theoretical treatment is given for achromatic trajectories (those for which the arrival point is insensitive to launch errors), and a method is presented to find them. This method is used in the elliptic restricted three-body problem to generate maps of key parameters associated with mass-catching near L_2. Catching strategies are considered, and equations are given for minimum-energy catcher maneuvering. The problem of optimal colony location is treated by consideration of operational aspects and of long-term numerical integrations via Cowell's method, in a planar restricted four-body problem. Optimal colony inclination is estimated via the method of phase equilibria. It is concluded that a 2:1 or 5:2 resonant orbit is preferable over alternatives of 3:1 or 7:3 resonances, and is markedly superior to L_5.

Introduction

This paper represents the third of a continuing series treating the detailed problems of large-scale transport of lunar mass for use in space colonization. Earlier contributions[1,2] outlined the major features of the methods and solutions which currently appear most promising. In particular, Ref. 1 (hereafter referred to as Paper I) gave the theoretical background for the developments to be presented here.

The mass-transport method selected involves launch by mass-driver (electromagnetic accelerator) of packages of lunar material, which follow ballistic trajectories to a catcher near L_2. Paper I treated these trajectories and showed the existence of a launch site for which the sensitivity, due to errors in launch velocity, is particularly low (formally, zero). The present paper presents new developments concerning trajectories from this site, systematically applying the results to the problem of mass-catcher operation. Paper I also proposed a new colony site: a 2:1 resonant orbit. The present paper considers the question of colony location in greater detail, confirming the advantages of the cited orbit and of a similar orbit, at the 5:2 resonance.

Achromatic Trajectories

It is possible to launch payloads, on ballistic trajectories, from the lunar surface to a selected point in space such that the miss distance at the target is effectively zero in the presence of nonzero errors in a selected component of launch velocity. The associated launch site is described as a critical point, and the resultant trajectories are described as achromatic. The existence of achromatic trajectories was first demonstrated by numerical computation on July 19, 1976. The terminology of "achromatic" is due to O'Neill [3] and derives from the action of achromatic lenses in focusing light of diverse wavelengths to a common focus, this action being due to the vanishing of a wavelength-dependant derivative (dispersion coefficient). The "focusing" action of achromatic trajectories results from the vanishing of a velocity-dependent derivative (sensitivity coefficient). In Paper I, it was shown that sensitivities due to errors in along-track velocity (V_T) are some 1000-5000 meters/mm/sec of launch error, which is up to two orders of magnitude larger than those due to errors normal to the track (V_N) and up to three orders larger than those due to cross-track (V_Z) errors, when the mass-driver track lies in the lunar equator. (These components are illustrated in Fig. 1.) Consequently, in what follows, only V_T-insensitive achromatic trajectories are considered.

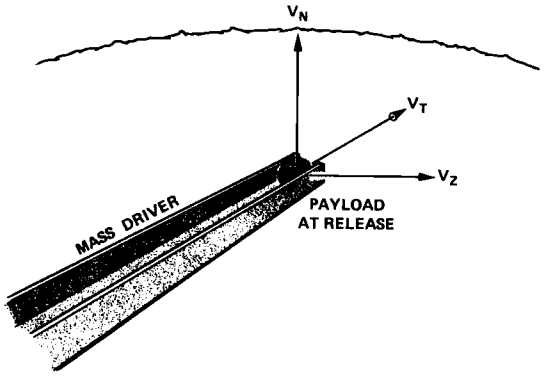

Figure 1. Components of launch velocity at release.

In Paper I, the existence and character of achromatic trajectories was considered using aspects of the topological properties of continuous mappings. However, much insight can be gained into their nature through consideration of two-body motion in a rotating coordinate system (Figure 2).

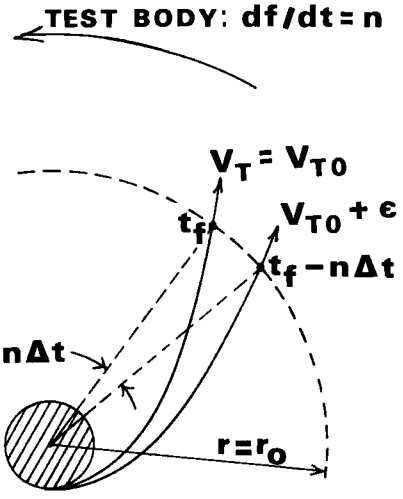

Figure 2. The physical character of achromaticity.

† Alexander von Humboldt Research Fellow. Member, AIAA

Consider a family of trajectories resulting from tangential launches from the surface of a planet. Let there be a test body in orbit, moving with angular velocity df/dt = n. Now consider a trajectory resulting from launch with velocity V_{T_o}, passing a distance $r = r_o$ from the planet center with flight time t_{f_o} and reaching $r = r_o$ at true anomaly $f = f_o$. Let the launch velocity suffer a perturbation: $V_T = V_{T_o} + \varepsilon$. Suppose that the perturbed trajectory passes $r = r_o$ with flight time $t_{f_o} - \Delta t_f$ and at true anomaly $f = f_o - n\Delta t_f$. Then, in a coordinate system rotating with the test body, the two trajectories would be seen to cross at distance r_o. If, following Paper I, we define a sensitivity coefficient

$$C_{VT} = \frac{\text{Miss distance}}{\Delta V_T} \quad \text{meters/mm/sec} \qquad (1)$$

In Paper I, the following was proved:

Theorem 1. The condition that $C_{VT} = 0$, for launch from longitude $\lambda = \lambda_o$, is that λ_o be the branch point joining two families of trajectories passing through $r = r_o$, one with $\partial\lambda/\partial V_T \leq 0$ and the other with $\partial\lambda/\partial V_T \geq 0$.

Figure 3 illustrates a numerical test of this theorem, for which the trajectories originate from the lunar surface and pass through L_2. We have $C_{VT} = 0$, very nearly, for $\lambda_o = 0.577768148$; the existence of the branch point is evident.

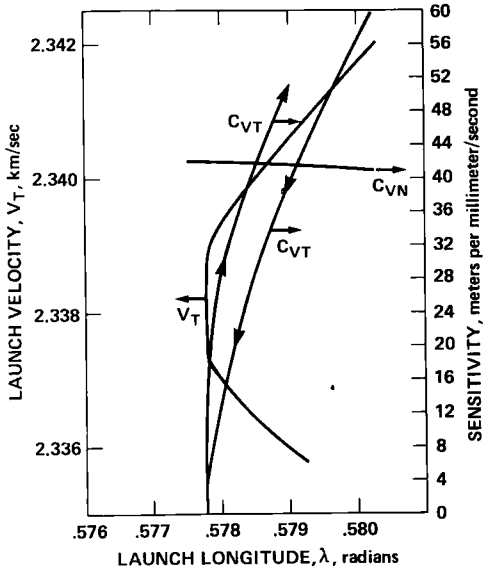

Figure 3. Application of Theorem 1 from Paper I.

We now prove the following:

Theorem 2. The two-body trajectory of Figure 2, for which $C_{VT} = 0$ at $r = r_o$, is unique.

Proof: This trajectory is a planar conic, defined uniquely by orbital elements a, e, $\tilde{\omega}$, f_o, where f_o is f at $r = r_o$. These quantities are determined by the following:

(1) $\tilde{\omega} = \lambda_o$ (launch site longitude)
(2) $a(1 - e) = r_p$ (planet radius)
(3) $a(1 - e^2)/(1 + e \cos f_o) = r_o$
(4) $n\,\partial t_f/\partial V_T = \partial f_{r=r_o}/\partial V_T$

Now with no loss of generality, let us define a target point P to lie at $r = r_o$ on the line joining the test body and planet center. We also define a longitude reference by specifying n = planet rotation rate. We now prove:

Theorem 3. The cited trajectory is such that for $V_T \geq V_{T_o}$, $\partial\lambda/\partial V_T \geq 0$ and for $V_T \leq V_{T_o}$, $\partial\lambda/\partial V_T \leq 0$.

Proof: For $V_T = V_{T_o}$, statement (4) of the proof of Theorem 3 implies $\partial\lambda/\partial V_T = 0$. For $V_T < V_{T_o}$ it is true that $n\partial t_f/\partial V_T > \partial f_{r=r_o}/\partial V_T$ so that for launch from longitude $\lambda = \lambda_o$, the trajectory reaches $r = r_o$ with $t_f > t_{f_o} + n\Delta t_f$ which is "too late" to hit P. Hence λ must be increased and $\partial\lambda/\partial V_T < 0$. For $V_T > V_{T_o}$ it is true that $\partial f_{r=r_o}/\partial V_T > n\partial t_f/\partial V_T$ so that for launch from λ_o, the trajectory reaches $r = r_o$ with $f < f_o - n\Delta t_f$ and the trajectory is "too flat" to hit P. Hence λ must be increased and $\partial\lambda/\partial V_T > 0$.

The cited nominal trajectory thus is achromatic, in the sense of Theorem 1 and of Paper I. We then have the following:

Theorem 4. The existence of achromatic trajectories follows from consideration of rotating coordinate systems and in no way depends on the specific properties of the restricted three-body problem or of any other dynamical model adopted.

This theorem is true because achromaticity is seen to represent a topological property of trajectories.

Theorem 5. Given a specified launch site, the focus point for an achromatic trajectory launched with given V_T is found by integrating two neighboring trajectories in an appropriate rotating coordinate system, launched tangentially with respective velocities V_T and $V_T + \varepsilon$, $\varepsilon \neq 0$ and $\varepsilon \ll V_T$. The focus point then is the point where the two trajectories cross.

Theorem 5 provides a means of constructing achromatic trajectories which is much more direct and simple than that of Paper I. That method involved a laborious repeated solution, by Newton iteration, of a two-point boundary value problem; consequently Paper I was able to treat only three isolated achromatic trajectories. In applying the method of Theorem 5, one must consider that trajectories are integrated numerically and are known, not as continuous curves, but as discrete specifications of state vectors printed out no more frequently than once each integration step.

Consequently, for integrations in the plane, let $(x_1, y_1, \dot{x}_1, \dot{y}_1)$ be the state vector for the trajectory launched at velocity V_T, $(x_2, y_2, \dot{x}_2, \dot{y}_2)$ the state vector for that launched with $V_T + \varepsilon$. Then near the focus point, there exist time increments Δt_1, Δt_2 such that

$$\begin{aligned} x_1 + \dot{x}_1\Delta t_1 &= x_2 + \dot{x}_2\Delta t_2 \\ y_1 + \dot{y}_1\Delta t_1 &= y_2 + \dot{y}_2\Delta t_2 \end{aligned} \qquad (2)$$

Then at each integration step, Δt_1 is computed and, providing the determinant $(\dot{x}_2\dot{y}_1 - \dot{x}_1\dot{y}_2) \neq 0$, the focus point lies between the two integration steps for which Δt_1 changes sign. It is then located more precisely by interpolation. The vanishing of the determinant is associated with a local parallelism of the two computed trajectories, so that by keeping

track of this quantity, one distinguishes between parallelism and crossing. It is also possible that Δt_1 and the determinant vanish simultaneously. This is associated with the two trajectories being locally tangent where they cross.

The geometry of the crossing is given in Figure 4. Here $\Delta\gamma$ is the angle at crossing and Δx is the deviation in the location of the crossing point from the catcher location. We have for the miss distance Δy:

$$\Delta y = \epsilon^2(\partial\Delta\gamma/\partial V_T)(\partial\Delta x/\partial V_T) \qquad (3)$$

which is quadratic in the launch velocity error. The ordinary situation, in which $\Delta y \propto \epsilon$, thus does not apply and one cannot regard the dispersion in impact points, due to errors in V_T and (for example) in V_Z, as giving rise to an error ellipse. Instead, the pattern of the impacts will lie within a curve shaped like the letter **D**. An approximately symmetrical error ellipse results only if allowed errors in V_T produce much less dispersion than allowed errors in V_N.

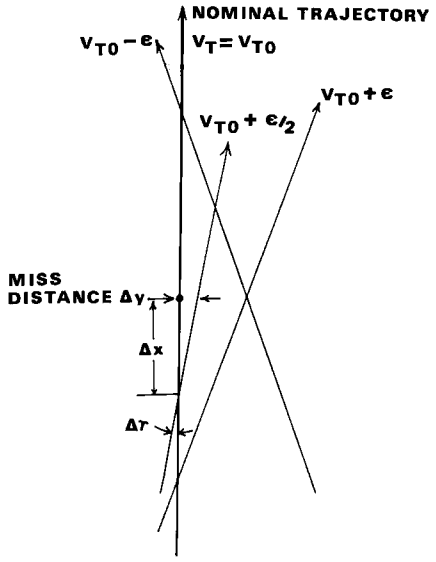

Figure 4. The geometry of a focus point.

The foregoing discussion applies to trajectories lying in the plane of the planet equator. For three-dimensional trajectories, it is not in general true that the analog of eqs. (2) possess solutions. However, Paper I showed that V_Z-errors give the least sensitive effects, 5 meters/mm/sec or less, so for approximately planar trajectories it will be seen that the principal effect of the out-of-plane motion is to limit the errors in V_T which otherwise would be allowed by eq. (3). It then is true that achromatic trajectories can result for large ranges of V_T and λ and for moderate ranges of launch latitude β. There then results, for all three of V_T, λ, β varying arbitrarily, a continuous volume of points each of which is a focus point for an achromatic trajectory.

In the present problem, β and λ are not considered to so vary. Rather, we consider a fixed mass-driver installation on the lunar surface, so that λ and β vary principally in response to the lunar librations in longitude and latitude. Hence, for time periods of the order of a month, the set of focus loci, associated with the fixed launch site, constitutes a cylinder (Figure 5). In what follows, we consider the mapping of parameters on such cylinders.

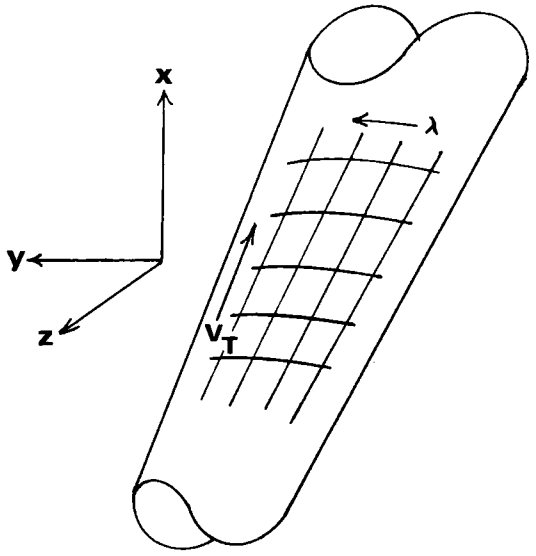

Figure 5. Representation of focus points as a mapping on a cylinder.

Lunar Mass Transport

The Lunar Motions

Discussions of lunar motions have been given in Ref. 4 and elsewhere. The following brief description presents those results needed for the present work.

The libration in latitude $\Delta\beta$ results from the lunar obliquity on its orbital plane, which has the constant value $6^o40'44"$. The libration in latitude has amplitude of approximately this value and period of one draconitic month (time between successive passages of the ascending node on the ecliptic) which is 27.212220 days.

The libration in longitude $\Delta\lambda$ results from the lunar eccentricity e_m and is given approximately by the difference, (mean anomaly) - (true anomaly):[5]

$$\Delta\lambda = -2[\beta'(1+\cos\phi)\sin f_m - \beta'^2(\tfrac{1}{2}+\cos\phi)\sin 2f_m + \beta'^3(\tfrac{1}{3}+\cos\phi)\sin 3f_m + \ldots]$$
$$\cos\phi = \sqrt{1-e_m^2} \qquad (4)$$
$$\beta' = \tan\phi/2 = \frac{1}{e_m}(1-\sqrt{1-e_m^2})$$

where f_m = lunar true anomaly. The period is one anomalistic month (time between successive passages of perihelion): 27.5545503 days. Consequently it is not true that $\Delta\lambda$, $\Delta\beta$ are in phase; their variations trace out a Lissajous curve. In any month, they trace out an ellipse which is geometrically proportional to the cross-section of the cylinder of Figure 5.

Further, e_m varies from 0.0432 to 0.0666 with mean of 0.0549. The principal contribution to this effect has period 206.26735 days and is known as the evection.

In all the rest of this paper, as in Paper I, the following normalized units are used: unit mass = (Earth + Moon), lunar mass = $\mu = 0.01215$, unit distance = 384,410 km, unit time = 104.362 hours, unit velocity = 1023.17 m/sec, unit acceleration = 0.00273 m/sec^2. The lunar radius $r_m = 0.00452133$.

Initially let us consider achromatic trajectories in the planar circular restricted three-body problem, the equations being given in Moon-centered coordinates:

$$\ddot{x} - 2\dot{y} = \Omega_x \qquad \ddot{y} + 2\dot{x} = \Omega_y$$

$$\Omega = \tfrac{1}{2}[(x + 1 - \mu)^2 + y^2] + (1 - \mu)/r_1 + \mu/r_2 \qquad (5)$$

$$r_1^2 = (x + 1)^2 + y^2 \qquad r_2^2 = x^2 + y^2$$

The achromatic trajectory of Figure 3 has its focus point, L_2, located at ($x = 0.167833$, $y = 0$) and originates with a due-east launch from $\lambda = 0.577768148$ with $V_T = 2.28268684$. Because the trajectory is achromatic, the last value is not critical. Hence as an initial test, eqs. (5) were integrated with the cited λ and with $V_T = 2.285$.

This integration, as well as all others of the type described here, was performed on the CDC 3300 terminal-operated computer of the Max-Planck-Institut für Kernphysik, in the 36-bit-word mode, which corresponds to carrying 10 to 11 significant figures in the computation. The integration step was 0.0001 for $r_2 < 3r_m$, 0.003 for greater r_2. Parallel integrations were performed upon two trajectories, both originating from the cited λ and with respective velocities V_T, $V_T + 0.001$; the focus point was found via eqs. (2). For the initial test integration, the focus point was determined numerically as ($x = 0.16778$, $y = 0.00002$), which accuracy was regarded as acceptable.

Because eqs. (5) are planar, the cylindrical representation of Fig. 5 reduces to a two-sided plane which is referred to as the "flat cylinder"; this terminology is used because maps of certain parameters, which will be exhibited, resemble perspective drawings of three-dimensional cylinders and must be distinguished from them. Figure 6 represents a map on the flat cylinder of focus points associated with several values of V_T and $\Delta\lambda$; values of $\Delta\lambda$ up to $\pm 8^0$ are taken, which from eqs. (4) represents the range in $\Delta\lambda$ due to the upper limit on e_m.

It is not the case that contours of constant $\Delta\lambda$ correspond to the traces of trajectories; this is obvious since each point on such a curve corresponds to a different value of V_T and hence has a distinct value of the Jacobi constant $C = -\frac{1}{2}(\dot{x}^2 + \dot{y}^2) + \Omega$. However, it is true that at each point on such a curve, the tangent to the curve coincides approximately with the tangent to the trajectory and hence indicates the direction of the mass-stream from the Moon. This results from the small angles with which the two computed trajectories cross.

It was earlier noted that there exist points for which the two trajectories are locally tangent while crossing. The locus of these points is found to coincide closely with the curve $V_T = 2.275$. At such points, the miss distance Δy is cubic in ε rather than being quadratic as in eq. (3). Points with $\Delta y \propto \varepsilon^4$ do not exist since they would result in the two trajectories coinciding throughout.

A variety of other variables were computed along the trajectories and mapped. Figure 7 gives contours of flight time and arrival velocity at the target point, mapped in coordinates x, y on the flat cylinder (dotted outline). This map emphasizes the distinction between trajectories and constant-λ focus loci, because V increases markedly with increasing x. Along a trajectory, by contrast, velocity decreases slightly with increasing x. The low-velocity focus points involve trajectories which curve back toward the Moon, rather than escaping.

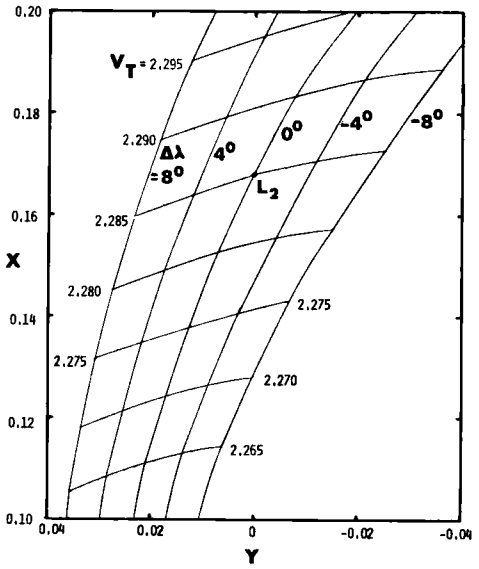

Figure 6. Map on the flat cylinder of focus loci associated with launch, $e_m = 0$

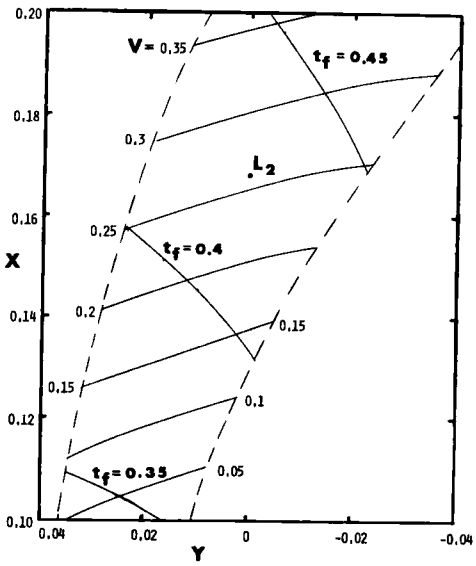

Figure 7. Map on the flat cylinder of flight time and arrival velocity, $e_m = 0$

For consideration of the effects of variation in launch site latitude, it is necessary to provide information on the miss sensitivity due to errors in launch z and V_Z, the associated coefficients being

defined as in eq. (1) and denoted (vide Paper I) C_Z and C_{VZ}. This information is provided by Figure 8. The variations in C_Z are seen to reflect the radial geometry of the problem, being close to the value of r_2 measured in units of r_m. Their negative values reflect the fact that trajectories launched initially tangent to the equator, with nonzero positive latitude, cross the equator at their descending nodes and subsequently possess ground tracks over lunar southern latitudes. But such an effect does not occur for C_{VZ}, for which the gradient is larger in magnitude. The curve $C_{VZ} = 0.0$ corresponds to trajectories which are achromatic with respect to errors both in V_T and V_Z.

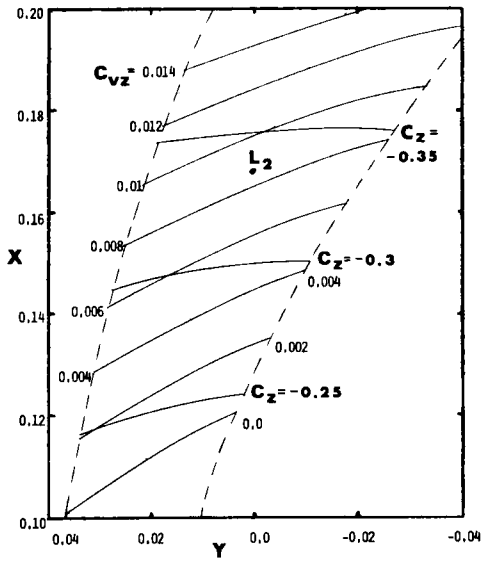

Figure 8. Map on the flat cylinder of C_Z and C_{VZ}, $e_m = 0$

These data were obtained by integrating eqs. (5) together with linearized out-of-plane variational equations:

$$\ddot{z}_{a,b} + z_{a,b}\left[\frac{1-\mu}{r_1^3} + \frac{\mu}{r_2^3}\right] = 0 \quad . \tag{6}$$

subject to initial conditions

$$z_a(0) = 1,\ \dot{z}_a(0) = 0,\ z_b(0) = 0,\ \dot{z}_b(0) = 1 \tag{7}$$

and C_Z, C_{VZ} are respectively the values of z_a, z_b at a focus point. Equation (6) would be the true out-of-plane equation of motion if, in eqs. (5), we took $r_1^2 = (x+1)^2 + y^2 + z^2$, $r_2^2 = x^2 + y^2 + z^2$. The neglect of the z^2 terms makes (6) linear in z so it is a variational equation and not an equation of motion.

Maps in the Elliptic Restricted Three-Body Problem

The shift in λ, associated with lunar libration in latitude, is a result of lunar eccentricity; hence it cannot be completely accounted for outside of a dynamical model which takes e_m explicitly into account. Such a model is given by the elliptic restricted three-body problem, and this model will then take account of virtually all perturbations on the trajectories, insofar as it was shown in Paper I that residual perturbations (solar effects) are quite small.

There is ordinarily no advantage in using the elliptic rather than the circular restricted problem, in preliminary investigations such as the present study. The equations are more complex, and the Jacobi integral does not exist as an algebraic function of the state-vector components. This last results from the explicit appearance of the independent variable f_m, the lunar true anomaly, in the equations of motion. Moreover, this appearance of f_m adds an additional degree of freedom to the system, insofar as an initial value must be specified. But for the present problem, it is possible to define a renormalization of the initial conditions at launch, such that these conditions are expressed uniquely and in a convenient manner, as functions of f_m which are related by physical considerations to the initial choice $f_m = 0$.

In what follows the in-plane coordinates x, y "pulsate", being normalized with respect to the variable Earth-Moon distance, and rotate at rate $df_m/d\ell_m$, ℓ_m = lunar mean anomaly:[6]

$$x = W\bar{x}\ ;\ y = W\bar{y}\ ;\ \frac{df_m}{d\ell_m} = W^2\sqrt{1 - e_m^2}$$
$$W = (1 + e_m \cos f_m)/(1 - e_m^2) \tag{8}$$

where $\bar{x}$, $\bar{y}$ are nonpulsating rotating coordinates. In what follows we use the mean value, $e_m = 0.0549$. Then equations of motion corresponding to (5) are given, with $(\ )' = d(\ )/df_m$:

$$x'' - 2y' = \Omega_x \qquad y'' + 2x' = \Omega_y$$
$$\Omega = (1 + e_m \cos f_m)^{-1}\{\tfrac{1}{2}[(x + 1 - \mu)^2 + y^2] + (1-\mu)/\rho_1 + \mu/\rho_2\} \tag{9}$$
$$\rho_1^2 = (x+1)^2 + y^2 \qquad \rho_2^2 = x^2 + y^2$$

and again L_2 exists and is located at ($x = 0.167833$, $y = 0$). Equations (9) were integrated subject to initial conditions defined as follows:

$$(f_m)_0 = n\pi/4,\ n = 0, 1, 2, \ldots 8$$
$$\lambda_0 = 0.577768148 + \Delta\lambda[(f_m)_0];\ \Delta\lambda = (\text{eq. } 4)$$
$$r_m = 0.00452133\ W_0\ ;\ W_0 = W[(f_m)_0]$$
$$x_0 = -\,r_m \cos\lambda_0;\ y_0 = -\,r_m \sin\lambda_0 \tag{10}$$
$$V_0 = 2.265 + 0.005\ m,\ m = 0, 1, 2, \ldots 8$$
$$x'_0 = [(V_0 \sin\lambda_0)W_0 + x_0 W'_0]/W_0^{\,k}$$
$$y'_0 = [(-\,V_0 \cos\lambda_0)W_0 + y_0 W'_0]/W_0^{\,k}$$
$$\text{and } W'_0 = -(e_m \sin (f_m)_0/(1 - e_m^2)$$

and k is chosen such that maps of parameters, akin to Figs. 6-8, may be generated for the selected values of $(f_m)_0$, V_0 so as to give not too large an effect due to $e_m \neq 0$. The value $k = 2.0$ was found by numerical experiment to give good results. Equations (10) then define the renormalized initial conditions, which permit study of eqs. (9) with virtually the same convenience as eqs. (5). It is important to note that the renormalization involves the initial conditions only and not the equations of motion; it is not possible to select dependent and independent variables which will reduce eqs. (9) to a simpler form than is provided by the standard choice, eqs. (8).[7] Moreover, eqs. (8) lead to the

standard normalization of velocities which is x', y' in eqs. (10) with k = 0. Since this standard normalization applies to velocities subsequent to launch, numerical designation of renormalized velocities will involve the suffix "R". Thus, "V_T = 2.285R" refers to an initial condition for which V_0 = 2.285; "V = 0.259" refers to a subsequent condition for which $(x'^2 + y'^2)^{1/2}$ = 0.259.

Figure 9 then is the counterpart of Figure 6, being a mapping onto the flat cylinder of focus loci for achromatic trajectories with cited values of V_0 and $(f_m)_0$. There is evident similarity to Fig. 4. The map is very evenly divided to the right and left of L_2, which confirms the suitability of the selected launch site. In reality, there is slight unevenness insofar as the loci with $(f_m)_0 = 0^0$, 180^0 pass respectively to the right and left of L_2 with miss distances of -0.00291, 0.00250. Hence a more accurately centered map would result by displacing the launch site eastward by 0.001221 radians or 2.123 km. Again it is found that there exists a locus of points where the pairs of computed orbits (respectively with renormalized launch velocities V_0 and V_0 + 0.001) are tangent while crossing, this locus lying close to the curve of V_T = 2.275R.

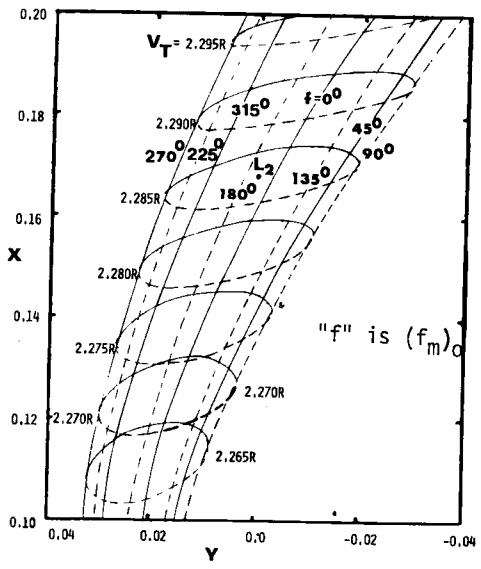

Figure 9. Same as Fig. 6 except e_m = 0.0549

Figure 10 is the counterpart of Fig. 7; the flight times t_f are the elapsed increase in f_m subsequent to launch. Figure 11 is the counterpart of fig. 8 and was found in the same way, except that the counterpart of eqs. (6) is written:[6]

$$z_{a,b}'' + z_{a,b}(1 + e_m \cos f_m)^{-1}(e_m \cos f_m + \frac{1-\mu}{\rho_1^3} + \frac{\mu}{\rho_2^3}) = 0 \qquad (11)$$

and $\rho_{1,2}$ are as in eq. (9) while eq. (11) is integrated with the initial conditions of eq. (7). In Fig. 11 it is again seen that there is a locus of foci for which trajectories are achromatic with respect to both V_T and V_Z, and which is close to the locus of this type in Fig. 8.

In Figures 9-11, there are no fundamental differences with respect to their counterparts. The elliptical nature of the loci reflects the additional degree of freedom associated with the choice of $(f_m)_0$. It is not possible to take out all of the associated variation without a rather more complex renormalization than eqs. (10), but merely to reduce the variation so as to prevent it from being a serious inconvenience.

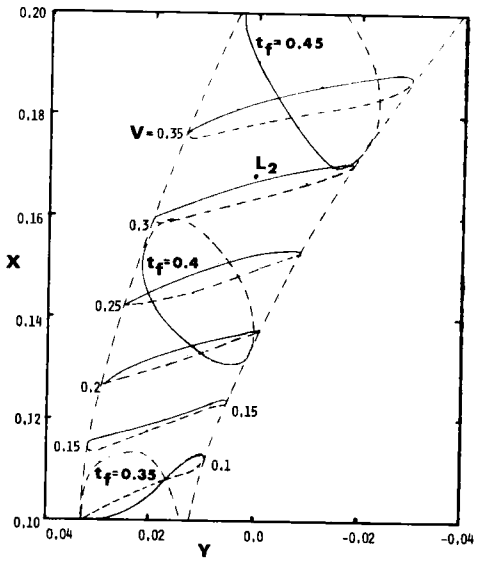

Figure 10. Same as Figure 7 except e_m = 0.0549.

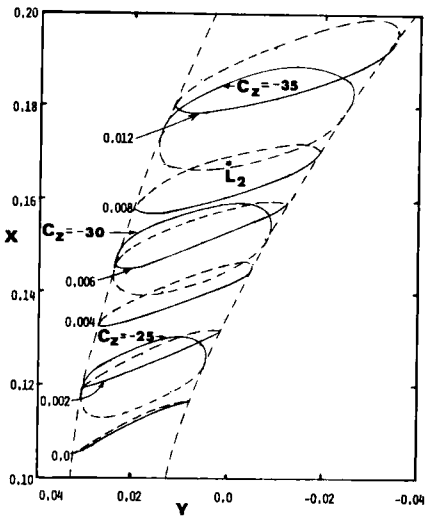

Figure 11. Same as Figure 8 except e_m = 0.0549.

System Applications

In consideration of engineering aspects of lunar mass transport, the mass-catcher has not been well defined but some attention has been given to concepts such as that of Figure 12. Representative features of this concept include:[8]

Target diameter ∿ 100 meters
Total capacity ∿ 100,000 tons
Empty mass ∿ 5000 tons
Fill time = 1 month
Onboard power ∿ 40 Mw
Onboard thrust ∿ 10^4 newtons (Isp = 405 sec.)

For purposes of the present discussion, the key considerations are its widely variable mass, its target diameter, its maneuver capability, and its capability for catching of high-velocity payloads. In what follows, we consider application of the results of the trajectory computations to the definition of design tradeoffs involving this catcher and the mass-driver, and to their operational use.

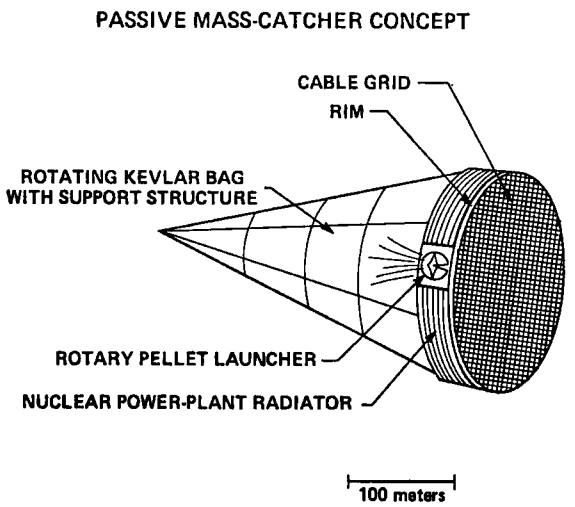

Figure 12. Mass-catcher concept

Mass-Driver Accuracy

The reported computations permit the assessment of requisite mass-driver accuracy. The data contains printouts of time histories of trajectory state vectors for values of V_T separated by $\varepsilon = 0.005$. By direct comparison of such neighboring trajectories one may derive the miss distances, Δy, eq. (3), with respect to computed focus points found with $\varepsilon = 0.001$. In practice one may treat values of Δy with $\varepsilon = +0.004$, $\varepsilon = -0.006$ and test eq. (3) by considering that the ratios of the two values of Δy should be approximately in the ratio $(6/4)^2$. This is found to be approximately true. In this manner the allowed variation in V_T is found to be correlated with arrival velocity V, fig. 7, and is given approximately by

$$\Delta V_T = \varepsilon = 0.06\left[(V/0.25)(\Delta y/40\ \text{m})\right]^{1/2}\ \text{m/sec} \qquad (12)$$

where 40 meters ($\sim 10^{-7}$) was taken as the reference scatter and Δy is fixed by the catcher design. Equation (12) holds for planar motion and requires modification for the effects of initial inclination of the motion at launch, with respect to the lunar equator, produced (for example) by lunar obliquity. Thus, if ψ is the inclination angle in radians, and taking $C_{VZ} = 0.01$ as reference value,

$$= \varepsilon\ 0.10\left(\frac{0.01}{C_{VZ}}\right)\left(\frac{\tan 0.1}{\tan \psi}\right)\left(\frac{\Delta z}{40\ \text{meters}}\right)\ \text{m/sec} \qquad (13)$$

and eq. (13) reflects the scatter in arrival z due to that component in ΔV_Z derived from a tangent-law association with ΔV_T; an additional component of scatter in z would follow from uncorrelated (intrinsic) variations in ΔV_Z at launch. For a due-east launch, with $\psi < 6.9^0$ due to lunar obliquity, eq. (12) may provide the limit on ε. It must also be noted that variations in ΔV_N must be held an order of magnitude lower than variations in ΔV_Z, owing to the correspondingly greater C_{VN} found in Paper I. Reference (2) proposed the intrinsic limits on allowed ΔV_N, ΔV_Z as respectively 0.01, 0.1 m/sec. But from an engineering standpoint the correction and control of ΔV_N, ΔV_Z are identical problems insofar as both errors are normal to the mass-driver track and to the initial flight path. Consequently, success in controlling ΔV_N will permit control of the intrinsic ΔV_Z such that virtually all ΔV_Z will arise as $\Delta V_Z = \Delta V_T \tan \psi$.

Mass-Driver Siting and Aim

From Fig. 9, the optimal site is defined as equatorial and lying at longitude $33^0 10'.42$ east. Such a site is associated with focus-locus maps, on the flat or three-dimensional cylinder, which are accurately centered on L_2 for mean e_m. Since the catcher motion is heavily constrained by such maps, any offset in the maps, from being centered at L_2, results in a continuous catcher acceleration being required to maintain the offset. More particularly, if Δx, Δy, Δz are the components of the offset,

$$\ddot{\Delta x} = 7.38084\ \Delta x\ ;\ \ddot{\Delta y} = -2.19042\ \Delta y\ ;\ \ddot{\Delta z} = -3.19042\ \Delta z \qquad (14)$$

are the required accelerations.

For use in site assessment and evaluation, there exists a considerable body of high-quality spacecraft photography of the cited location and its environs, including:

Lunar Orbiter: I-41M, I-42M, I-48M, I-49M, IV-73H$_1$, V-55M to V-63M, V-55H to V-63H
Apollo mapping camera: AS15-2546 to -2548 and AS15-2680 to -2687

Figure 13 (LO IV-73H$_1$) shows the site as lying near the north rim of the crater Censorinus, in rugged country. Figure 14 (LO V-63M), an oblique view, shows that the proposed site has several unfavorable features. It lies atop a ridge almost due north of Censorinus and just to the west of the high crater wall of Maskelyne-A. Consequently it is not possible to launch tangentially without striking this wall which is elevated above the surrounding terrain. Moreover, an oblique launch would give the effect of a westward shift in the launch site and by eq. (14) would thus produce a major catcher offset. These photographs further show that the rugged, unfavorable terrain and the Maskelyne crater wall extend north for at least a degree of latitude, while to the south the terrain appears even more rugged and crater-pocked.

However, Fig. 13 suggests that much more favorable conditions exist in the V-shaped bay of Mare Tranquillitatis lying due north of Maskelyne-A. Figure 15 (LO I-48M) confirms that this location represents typical mare terrain, moderately cratered but free of major eminences--altogether, as satisfactory a site as might be expected. The coordinates of the proposed site are approximately $33^0 40'$ east by $1^0 44'$ north. The associated offsets at L_2 are $\Delta y = 0.00146$, $\Delta z = -0.005077$ with associated ΔV requirements to maintain the offset of $\dot{\Delta y} = 0.0202$, $\dot{\Delta z} = 0.1018$ per month.